INTERNATIONAL JOURNAL OF HYDROGEN ENERGY 37 (2012) 8428–8438

Available online at www.sciencedirect.com

SciVerse ScienceDirect

journal homepage: www.elsevier.com/locate/he

A mixed-cation mixed-anion borohydride $NaY(BH_4)_2Cl_2$

Dorthe B. Ravnsbæk [a], Morten B. Ley [a], Young-Su Lee [b], Hans Hagemann [c], Vincenza D'Anna [c], Young Whan Cho [b], Yaroslav Filinchuk [a,d,1], Torben R. Jensen [a,*]

[a] Center for Materials Crystallography (CMC), Interdisciplinary Nanoscience Center (iNANO) and Department of Chemistry, University of Aarhus, Langelandsgade 140, DK-8000 Aarhus C, Denmark

[b] Materials/Devices Division, Korea Institute of Science and Technology, Seoul 136-791, Republic of Korea

[c] Department of Physical Chemistry, University of Geneva, 1211 Geneva, Switzerland

[d] Swiss-Norwegian Beam Lines at ESRF, BP-220, 38043 Grenoble, France

ARTICLE INFO

Article history:
Received 11 November 2011
Received in revised form
22 February 2012
Accepted 24 February 2012
Available online 27 March 2012

Keywords:
Hydrides
X-ray diffraction
Solid state structure
Solid phase synthesis
Transition metal

ABSTRACT

A new sodium-yttrium borohydride-chloride, $NaY(BH_4)_2Cl_2$, is obtained by a combination of mechanochemical synthesis and annealing of $NaBH_4$–YCl_3 mixtures and is characterized by *in-situ* synchrotron radiation X-ray powder diffraction, density functional theory, thermal analysis and vibrational spectroscopy. Several simultaneous and coupled reactions occur during the synthesis, also yielding Na_3YCl_6 and $Na(BH_4)_{1-x}Cl_x$ besides the title compound. The polymeric pseudo-orthorhombic crystal structure of $NaY(BH_4)_2Cl_2$ (space group *P2/c*) is built of edge- and corner-sharing octahedral coordination polyhedra of yttrium ($4Cl + 2BH_4$) and sodium ($2Cl + 4BH_4$). The structure is isomorphous to the high temperature polymorph of $NaYCl_4$. The BH_4 units in $NaY(BH_4)_2Cl_2$ are located only on the larger of the two independent anion sites in $NaYCl_4$. Density functional theory optimization of the experimental structure suggests that the BH_4 units act as η^3-ligands (face-sharing) towards yttrium and η^1-ligands (corner-sharing) towards sodium. Raman spectroscopy confirms this BH_4 configuration. $NaY(BH_4)_2Cl_2$ decomposes at ~300 °C under formation of Na_3YCl_6, while the latter compound at higher temperatures reacts with $Na(BH_4)_{1-x}Cl_x$ to form NaCl and possibly amorphous products. The reactions are associated with mass losses of 2.62 and 3.78 wt% for the $NaBH_4$–YCl_3 (3:1) and (4:1) samples, respectively.
Copyright © 2012, Hydrogen Energy Publications, LLC. Published by Elsevier Ltd. All rights reserved.

1. Introduction

The transition towards a sustainable and environmentally friendly energy system capable of meeting the increasing energy demands is considered one of the greatest challenges in the 21st century. Hydrogen is suggested as a future carrier of renewable energy, however a safe, compact and efficient hydrogen storage method still remains to be identified [1,2]. The metal borohydrides currently receive increasing interest as potential hydrogen storage materials due to their high hydrogen densities. Unfortunately, many of the well-known borohydrides exhibit poor thermodynamic and kinetic properties, which hamper their utilization in technological applications [3,4].

Recently, several new mixed-metal borohydrides have been synthesized and characterized, and some of these have

* *Corresponding author*. Tel.: +45 8942 3894; fax: +45 8619 6199.
E-mail address: trj@chem.au.dk (T.R. Jensen).

[1] Present address: Institute of Condensed Matter and Nanosciences, Université Catholique de Louvain, Place L. Pasteur, B-1348, Louvain-la-Neuve, Belgium.

0360-3199/$ – see front matter Copyright © 2012, Hydrogen Energy Publications, LLC. Published by Elsevier Ltd. All rights reserved.
doi:10.1016/j.ijhydene.2012.02.130

improved thermodynamic and kinetic properties, for example, $MSc(BH_4)_4$ (M = Li, Na or K) is found to decompose at temperatures below ~200 °C [5–8]. This is a significant lowering of the decomposition temperature as compared to the corresponding values for the alkali metal borohydrides, MBH_4, which decompose at approximately 380, 400 and 500 °C, for M = Li, Na and K, respectively [9].

Another new method for modification of structure and properties of known metal borohydrides is anion substitution, i.e. alkali or alkali earth halide salts forming solid solutions with corresponding borohydrides. This has recently been demonstrated for e.g. $LiBH_4$–LiX and $Ca(BH_4)_2$–CaX_2 (X = F, Cl, Br or I) [10–14].

The primary building unit in borohydrides is the BH_4^- tetrahedra, which can coordinate to metal atoms via a corner, edge or face, i.e. act as a η^1-, η^2- or η^3-ligand. This gives rise to a variety of molecular geometries and structure types. Metal borohydrides such as $Al(BH_4)_3$, $Zr(BH_4)_4$, and $Hf(BH_4)_4$ form molecular compounds, whereas, for example, $Mg(BH_4)_2$ and $Ca(BH_4)_2$ form three-dimensional network structures [15–19]. Furthermore, the recent studies of alkali metal–zinc borohydrides have demonstrated that mixed-cation borohydrides exhibit a variety of new stoichiometries and structural topologies, e.g. $LiZn_2(BH_4)_5$ and $NaZn_2(BH_4)_5$ are built of two identical interpenetrated three-dimensional frameworks, containing the $[Zn_2(BH_4)_5]^-$ anion, whereas $NaZn(BH_4)_3$ consists of a single three-dimensional network, possibly containing anions with the composition $[Zn(BH_4)_3]^-$ [20,21]. A bimetallic heteroleptic borohydride, $KZn(BH_4)Cl_2$ has also been structurally characterized recently and was found to contain a heteroligand anion $[Zn(BH_4)Cl_2]^-$ [22]. Combination of zinc and alkali metals in the mixed-metal compounds is fruitful in terms of tuning hydrogen storage properties. The zinc-based borohydrides prepared up to now are stabilized by alkali borohydrides and all have decomposition temperatures in the range from 95 to 127 °C [20–22]. Unfortunately, zinc is readily reduced during decomposition to its metallic form and diborane and hydrogen are released. Hence, lithium zinc borohydride can be used as a safe and convenient source of diborane e.g. for synthesis of other borohydrides [23–25]. Structural studies of novel bimetallic or heteroleptic borohydrides might hold the key to gain further insight into trends in the thermal stability and mechanisms of decomposition for bimetallic borohydrides.

Here, we present the solid state synthesis, crystal structure and the thermal decomposition for a novel mixed-cation mixed-anion borohydride, $NaY(BH_4)_2Cl_2$, studied by *in-situ* synchrotron radiation powder X-ray diffraction (SR-PXD), Raman and infrared spectroscopy, density functional theory (DFT) calculations, thermogravimetric analysis (TGA) and differential scanning calorimetry (DSC).

2. Experimental

2.1. Synthesis

The samples (1.102 and 1.115 g) were prepared from $NaBH_4$ and YCl_3 mixed in the molar ratios 3:1 and 4:1. The chosen compositions reflect the initial aim of this study, namely to synthesize a sodium-yttrium-borohydride analogue to the series of materials $MSc(BH_4)_4$ (M = Li, Na and K) [5–8]. All samples were ball-milled by high energy ball milling using a Pulverisette no. 4 with 80 mL tungsten carbide (WC) vials and five 10 mm balls. A sample/ball ratio of approximately 1:35 was used. The ball milling was performed under argon for 60 × 2 min, each interrupted by breaks of 2 min to avoid heating of the sample. The speed of the main disk during milling was 200 rounds per minute (rpm), while the speed of the milling planets was 560 rpm. For comparison a sample of $NaBH_4$–NaCl (1:1) was prepared using the same ball milling settings. The chemicals used were $NaBH_4$ (99.99%, Aldrich), YCl_3 (99.99%, Aldrich) and NaCl (99.99%, Aldrich). All handling and manipulation of the chemicals were performed in an argon-filled glove box with a circulation purifier.

2.2. Laboratory X-ray powder diffraction (PXD)

All samples were initially investigated using in-house powder X-ray diffraction (PXD) in order to identify the reaction products and estimate the crystallinity of the samples. PXD measurements were performed in Debye-Scherrer transmission geometry using a Stoe diffractometer equipped with a curved Ge(111) monochromator (Cu $K\alpha_1$ radiation) and a curved position sensitive detector. Data were collected at room temperature (*RT*) between 4 and 127° 2θ with counting time of ~960 s per step. Air-sensitive samples were mounted in a glove box in 0.4 mm glass capillaries sealed with glue.

2.3. Thermal analysis

Simultaneous thermogravimetric analysis (TGA) and differential scanning calorimetry (DSC) were performed using a Netzsch STA449C Jupiter instrument (*RT* to 500 °C, heating rate 10 °C/min) and corundum crucibles with lid as sample holder. The experiments were conducted in a helium (4.6) atmosphere.

2.4. In-situ time resolved synchrotron powder diffraction (SR-PXD)

In-situ SR-PXD data were collected both at the Swiss-Norwegian Beam Lines (SNBL) at the European Synchrotron Radiation Facility (ESRF) in Grenoble, France and at the beam lines I711 and I911-5 of the synchrotron MAX II, Lund, Sweden at the research laboratory MAX-lab [26,27].

At the ESRF a glass capillary (o.d. 0.5 mm) containing the sample was heated from *RT* to 230 °C at a rate of 2 °C/min, while SR-PXD data were collected [28]. The temperature was controlled with an Oxford Cryostream 700+. The data were collected using a MAR345 image plate detector at a sample to detector distance of 250 mm, and a selected X-ray wavelength of $\lambda = 0.732538$ Å. The capillary was oscillated 20° during X-ray exposure for 20 s.

At MAX-lab a specially developed sample cell for studies of gas/solid reactions was used, which allows high pressure and temperature to be applied [28]. The powdered sample was mounted in a sapphire (Al_2O_3) single-crystal tube (o.d. 1.09 mm, i.d. 0.79 mm). The sample was heated from *RT* to 350 or 500 °C with a heating rate of 7 °C/min. The temperature was

controlled with a thermocouple placed in the sapphire tube 1 mm from the sample. The data were collected using a MAR165 CCD detector system and selected wavelengths of $\lambda = 0.9550$ and 0.9077 Å at I711 and I911-5, respectively. The X-ray exposure time was 30 s.

All obtained raw images were transformed to 2D-powder patterns using the FIT2D program, which was also used for calibration using the PXD measurements of the standard NIST LaB_6 sample and masking diffraction spots from the single-crystal sapphire sample holder [29]. Uncertainties of the integrated intensities were calculated at each 2θ-point by applying Poisson statistics to the intensity data, considering the geometry of the detector [30].

2.5. Structure solution

Data collected at the ESRF for the $NaBH_4$–YCl_3 (3:1) sample at ~230 °C, containing the highest fraction of the new compound $NaY(BH_4)_2Cl_2$, was used for indexing and structure solution. Besides the main phase, the sample also contained sodium yttrium chloride, Na_3YCl_6 (space group $R-3H$) [31] and a solid solution of sodium borohydride–sodium chloride, $Na(BH_4)_{1-x}Cl_x$. The diffraction peaks from $NaY(BH_4)_2Cl_2$ were indexed by Dicvol [32] in a primitive orthorhombic cell ($a = 8.213$, $b = 6.815$ and $c = 6.671$ Å). However, the structure could not be solved in any orthorhombic space group, therefore a lower, monoclinic, symmetry was tested by global optimization in the direct space, using the program FOX [33]. The structure was ultimately solved in the space group $P2/a$, optimizing positions of one Y, one Na and one Cl atom and of a rigid tetrahedral BH_4 group and using a number of anti-bump restraints. The symmetry check in Platon did not show higher metric or crystallographic symmetry [34]. In order to make an easy comparison with the isomorphous compound $NaYCl_4$ (see below), the space group setting for the $NaY(BH_4)_2Cl_2$ was changed to the pseudo-orthogonal $P2/c$ (the standard setting of $P2/a$).

2.6. First-principles calculations

The experimental structure was re-optimized with first-principles calculations. The calculations were performed using density functional theory (DFT), as implemented in the Vienna Ab-Initio Simulation Package [35]. The generalized-gradient approximation by Perdew, Burke, and Ernzerhof is adopted for exchange-correlation functional [36]. Projector augmented wave potential with a plane wave cut-off energy of 500 eV is used [37]. A unit cell containing two formula units of $NaY(BH_4)_2Cl_2$ is used, and Monkhorst-Pack $4 \times 4 \times 4$ k-point meshes are sampled for the integration in the first Brillouin zone. The structures are optimized until the force on each atom becomes smaller than 0.005 eV/Å.

In order to verify that the final structure of $NaY(BH_4)_2Cl_2$ is the energetically most stable within the given symmetry, three structures with different initial orientations of the BH_4 group were made from joint optimization in FOX [33] against the data and three different sets of anti-bump restraints maximizing H–H and Cl–H distances. All three initial configurations converged during the theoretical optimization to an identical final structure (for atomic coordinates see Supplementary Table S3). The structural positions of Na, Y, B and Cl atoms agree well between the experiment and calculation.

The optimized $NaY(BH_4)_2Cl_2$ structure was further studied in order to determine why the BH_4 units are only positioned on the Cl2 site in the isomorphous $NaYCl_4$ structure ($MgWO_4$-structure type). The latter contains two crystallographically independent Cl sites, Cl1 and Cl2 (see Fig. 3). A DFT optimization was performed for the $NaYCl_4$-structure starting with the experimentally determined atomic positions for the isomorphous $NaErCl_4$ [38]. The atomic coordinates of the DFT optimized $NaYCl_4$-structure are shown in supplementary information as Table S4. Subsequently, a hypothetical structure was made in which all Cl atoms at the Cl1 site were fully replaced by BH_4 units. Starting from more than twenty different initial BH_4 orientations, the cell parameters and atomic coordinates were optimized within the $P2/c$ symmetry (for atomic coordinates see Supplementary Table S5).

In order to investigate possible Cl substitution on the BH_4 position in $NaY(BH_4)_2Cl_2$, crystal structures and total energies of $NaY(BH_4)_{2(1-x)}Cl_{2(1+x)}$ ($x = 0.0, 0.25, 0.5, 0.75, 1.0$) were calculated using a simulation cell constructed by replacing from 0 to 2 BH_4 units with Cl per formula unit.

2.7. Structural refinement

A final refinement of the DFT optimized $NaY(BH_4)_2Cl_2$ structure was performed against the SR-PXD data by the Rietveld method in the space group setting $P2/c$ using the program Fullprof [39]. All atomic positions were refined, including the positions of the rigid tetrahedral BH_4 group, however not its orientation (for atomic coordinates see Supplementary Table S1). The refinements indicate that one anion position is fully occupied by chloride and the second predominantly by the borohydride anion. However, an incorporation of 21(3) and 30(2) mol% Cl on the BH_4 site in $NaY(BH_4)_2Cl_2$ for the $NaBH_4$–YCl_3 (3:1) and (4:1) samples, respectively, is detected. The refinement also revealed 24.0(12) and 21.9(9) mol% Cl substitution on the BH_4 site in $NaBH_4$, present as a second phase in the $NaBH_4$–YCl_3 (3:1) and (4:1) samples, respectively. The background was described by linear interpolation between selected points. The refined unit cell parameters at ~230 °C for the three compounds in the $NaBH_4$–YCl_3 (3:1) sample are for $NaY(BH_4)_{1.58}Cl_{2.42}$ $a = 6.6649(4)$, $b = 8.2058(5)$, $c = 6.8109(4)$ Å, $\beta = 89.959(8)^\circ$, $Z = 2$, for Na_3YCl_6 $a = 7.1514(7)$, $c = 19.222(2)$ Å, $Z = 3$ and for $Na(BH_4)_{0.76}Cl_{0.24}$ $a = 6.1713(5)$ Å, $Z = 4$. The agreement factors are: R_{wp} (not corrected for background) = 3.62% and R_p (corrected for background) = 8.67% (See Rietveld refinement profile in Fig. 2). Furthermore, a Rietveld refinement was performed for the SR-PXD data measured at RT for the as-milled sample to extract the unit cell parameters of $NaY(BH_4)_2Cl_2$ at RT. These were found to be $a = 6.52(2)$, $b = 8.12(2)$, $c = 7.06(2)$ Å and $\beta = 88.1(2)^\circ$. Due to the poor crystallinity in the as-milled sample the exact sample composition and potential substitution degrees cannot be reliably determined.

2.8. Raman and infrared (IR) spectroscopy

Raman spectra were obtained on the ball-milled samples $NaBH_4$–YCl_3 (3:1) and (4:1) using a Kaiser Holospec Monochromator in conjunction with a liquid nitrogen cooled CCD

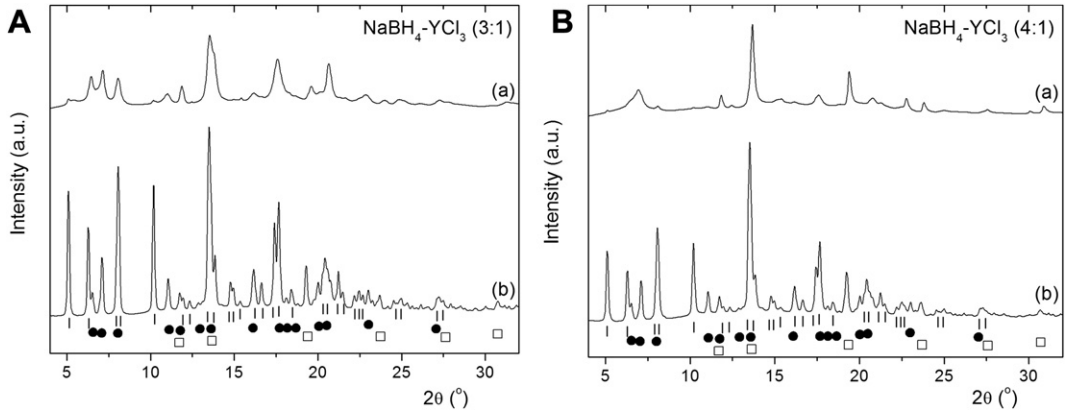

Fig. 1 – SR-PXD data for ball-milled samples of $NaBH_4$–YCl_3 (A) (3:1) and (B) (4:1). The data is measured at *RT* (a) and ~230 °C (b) (λ = 0.732538Å, BM01A, ESRF). Symbols: black lines $NaY(BH_4)_2Cl_2$, black circles Na_3YCl_6 and white squares $Na(BH_4)_{1-x}Cl_x$.

camera. Spectra were excited using the laser wavelength 488 nm with a typical laser power of 50 mW. The spectral resolution of the Raman spectra is about 3 cm^{-1}. The samples were sealed in melting point capillaries. High temperature experiments up to ca 180 °C were done by placing the capillary into a copper block connected to a circulating bath thermostat.

IR spectra were measured using a Bio-Rad Excalibur instrument equipped with a Specac low temperature Golden Gate diamond ATR system. The spectral resolution was set to 1 or 2 cm^{-1} for the different experiments. Samples were loaded in the glove box in the ATR system.

3. Results and discussion

3.1. *Synthesis, phase analysis and formation reaction pathways*

Sodium yttrium borohydride chloride, $NaY(BH_4)_2Cl_2$ was synthesized by a mechanochemical method, i.e. by ball milling of $NaBH_4$ and YCl_3 in compositions (3:1) and (4:1). The SR-PXD data collected at *RT* for the ball-milled samples show diffraction peaks from a small amount of $NaY(BH_4)_2Cl_2$, and apparently larger amounts of Na_3YCl_6 and a solid solution of sodium chloride–sodium borohydride, $Na(BH_4)_{1-x}Cl_x$. The relatively small amount of $NaY(BH_4)_2Cl_2$ formed during ball milling is insufficient for structural investigation of the novel compound from the diffraction data measured on the as-synthesized sample. Fortunately, the amount of $NaY(BH_4)_2Cl_2$ increases significantly as well as the overall crystallinity of all the compounds, as the sample is heated to ~230 °C during an *in-situ* SR-PXD experiment (see Fig. 1). Similar, observations have been made for a ball-milled sample of $Y(BH_4)_3$, $NaBH_4$ and LiCl in molar ratio 1:1:3 yielding $NaY(BH_4)_2Cl_2$ upon heating to 165 °C [40].The composition of the sample $NaBH_4$–YCl_3 (3:1) at ~230 °C was determined by Rietveld refinement (see Fig. 2) to be $NaY(BH_4)_{1.58}Cl_{2.42}$ (54.3(10) wt%, 28.4(5) mol%), Na_3YCl_6 (21.7(5) wt%, 6.77(16) mol%) and $Na(BH_4)_{0.76}Cl_{0.24}$ (24.0(12) wt%, 65(3) mol%). For the sample $NaBH_4$–YCl_3 (4:1) significantly smaller amounts of $NaY(BH_4)_{1.40}Cl_{2.60}$ (42.9(10) wt%, 16.4(4) mol%) and Na_3YCl_6 (17.9(5) wt%, 4.15(11) mol%) are formed, while more $Na(BH_4)_{0.78}Cl_{0.22}$ (39.2(16) wt%, 80(3) mol%) is observed. These results suggest that a starting composition of $NaBH_4$–YCl_3 (3:1) is more optimal compared to (4:1) and that excess amounts of $NaBH_4$ suppress the formation of Na_3YCl_6.

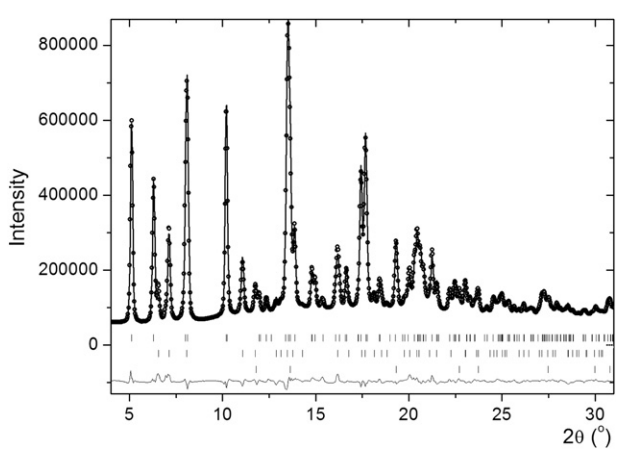

Fig. 2 – Rietveld refinement profile of SR-PXD data measured at 230 °C for the sample of $NaBH_4$–YCl_3 (3:1) (λ = 0.732538 Å, BM01A, ESRF). The sample contains $NaY(BH_4)_2Cl_2$ (top), Na_3YCl_6 (middle) and $Na(BH_4)_{1-x}Cl_x$ (bottom).

The sample compositions suggest that a series of simultaneous and coupled reactions takes place as described by Eqs. (1)–(3):

$$2NaBH_4 + YCl_3 \rightarrow NaY(BH_4)_2Cl_2 + NaCl \quad (1)$$

$$3NaCl + YCl_3 \rightarrow Na_3YCl_6 \quad (2)$$

$$1 - x\ NaBH_4 + x\ NaCl \rightarrow Na(BH_4)_{1-x}Cl_x \quad (3)$$

The two latter reactions are the competing addition reactions, whereas the formation of $NaY(BH_4)_2Cl_2$ takes place via a more complex pathway, possibly by a combination of metathesis and addition reactions. Diffraction peaks from NaCl were not observed in any of the samples, however the formation of Na_3YCl_6 and of the solid solution, $Na(BH_4)_{1-x}Cl_x$

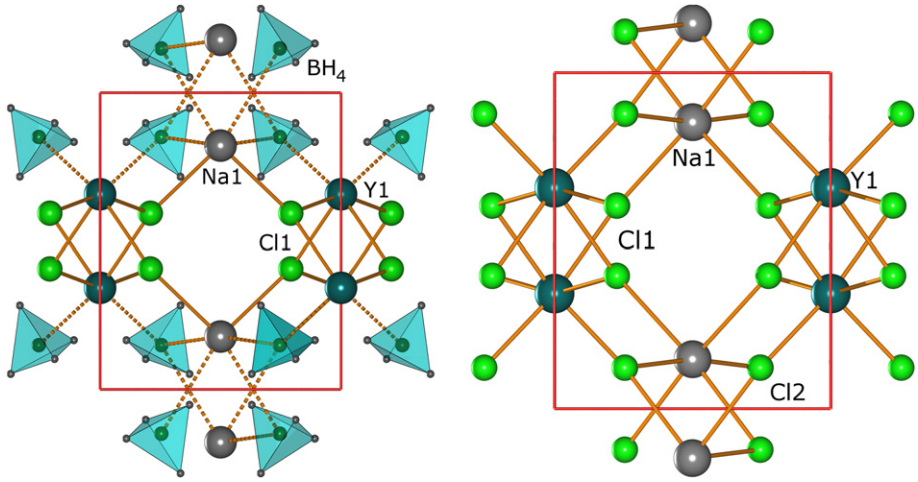

Fig. 3 – Crystal structures of $NaY(BH_4)_2Cl_2$ at $T \sim 230$ °C (left) and $NaYCl_4$ (right) viewed along [0 0–1].

indicates that NaCl is formed as an intermediate via Eq. (1) and that reactions (1) and (2) proceed at similar rates. In contrast, the simultaneous formation of $MSc(BH_4)_4$ and M_3ScCl_6 (M = Na or K) occurs without dissolution of MCl into MBH_4 [7,8], suggesting that the reaction corresponding to Eq. (2) is dominating for scandium, i.e. the formed MCl is consumed by fast formation of M_3ScCl_6, which prevents the dissolution of MCl in MBH_4. It should be noted, that that the Na_3YCl_6 (space group R-3) formed during the synthesis of $NaY(BH_4)_2Cl_2$ is a low temperature polymorph, which is reported to transform at $T = -30$ °C into the polymorph Na_3YCl_6 (space group $P2_1/n$) normally observed at ambient conditions [31]. Heating the sample to ~230 °C, does not induce this polymorphic phase transition. This may suggest that the chemical composition of the synthesised Na_3YCl_6 is slightly different and may include small amounts of BH_4 which replace chloride ions in the structure. It is also interesting that ball milling of $LiBH_4$–YCl_3 samples result in only a single metathesis reaction yielding $Y(BH_4)_3$ and LiCl. Thus, Li has apparently lower ability to stabilize double cation borohydrides and chlorides with yttrium [41–45]. Diffraction peaks from $Y(BH_4)_3$ have not been observed in this study.

3.2. *Crystal structure of $NaY(BH_4)_2Cl_2$*

$NaY(BH_4)_2Cl_2$ is found to crystallize in a primitive monoclinic unit cell with space group symmetry $P2/c$. The unit cell is only slightly distorted from the orthorhombic metrics, with a monoclinic angle $\beta = 89.959(8)°$. The sodium and yttrium atoms in the structure are located on the 2-fold rotation axis, while chloride and boron are on the general positions (see Fig. 3, left). The hydrogen positions were subsequently determined by DFT calculations and the resulting structure was refined by the Rietveld method (see Fig. 2).

Yttrium and sodium atoms both have slightly distorted octahedral coordination environments (see Fig. 4) made of two BH_4 units and four Cl atoms for yttrium (i.e. $Y(BH_4)_2Cl_4$) and of two Cl atoms and four BH_4 units for sodium atoms (i.e. $Na(BH_4)_4Cl_2$). The Cl atoms are coordinated in a trigonal planar fashion to one Na and two Y atoms, while the trigonal planar

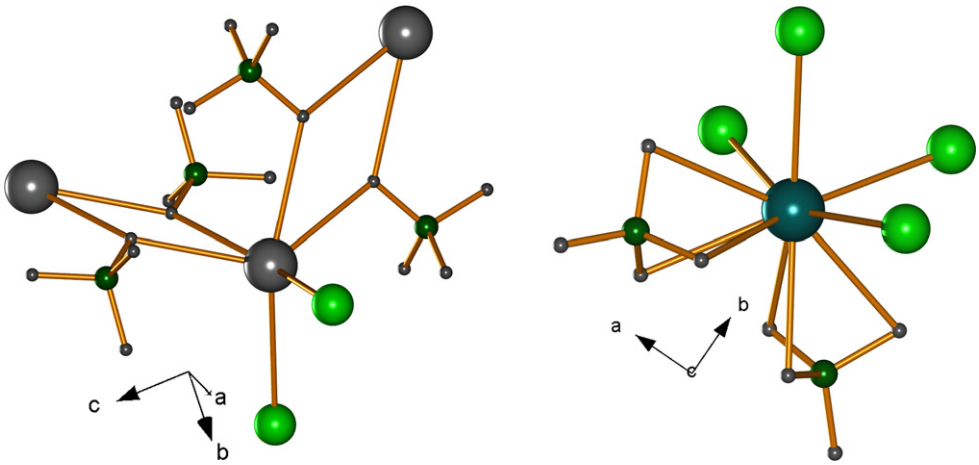

Fig. 4 – Coordination of Y atoms (left) and Na atoms (right) by BH_4 tetrahedra and Cl atoms in the $Y(BH_4)_2Cl_4$ and $Na(BH_4)_4Cl_2$ polyhedrons.

coordination of the BH_4 units is made by one Y and two Na atoms. Similar trigonal planar coordination has also been found for one of the BH_4 unit in β-$Ca(BH_4)_2$, $NaSc(BH_4)_4$, $NaZn(BH_4)_3$ and $KZn(BH_4)Cl_2$ [7,16,21,22]. Overall, the $NaY(BH_4)_2Cl_2$ structure is polymeric with the coordination polyhedra of the metal atoms sharing either corners or edges.

The Y–B distance of 2.529(13) Å in $NaY(BH_4)_2Cl_2$ is somewhat shorter than 2.714(11)–2.732(11) Å found for Y–B distances in the $Y(BH_4)_3$ polymorphs. This is in agreement with the bidentate BH_4–Y coordination in $Y(BH_4)_3$ expectedly being longer than the tridentate BH_4–Y coordination in $NaY(BH_4)_2Cl_2$ [41–43,46]. The Y–B distances found in $Y(BH_4)_3$ are closer to the Y–Cl distances found in $NaY(BH_4)_2Cl_2$ of 2.720(5)–2.725(6) Å. However, the Y–Cl distances are significantly longer than the Y–Cl distances found in YCl_3 of 2.585–2.638 Å [47]. Furthermore, the Y–Cl distances in the DFT optimized structure of the isomorphous compound, $NaYCl_4$ range from 2.528 to 2.716 Å, thus resembles both the Y–B and Y–Cl distances in $NaY(BH_4)_2Cl_2$, i.e. the distances are somewhat preserved. The angles around yttrium in $NaY(BH_4)_2Cl_2$ range from 76.64(14) to 100.2(3)°, increasing in the order Cl–Y–Cl < Cl–Y–B < B–Y–B. The bond distances around the sodium atoms are 2.924(9) and 2.919(13)–3.305(16) Å for Na–Cl and Na–B, respectively. The latter distances compare well with the Na–B distances found in $NaBH_4$ of 3.075 Å [48]. The bond angles around the sodium octahedron range from 71.0(2) to 100.37(14)°, however the angles are found to increase in reverse order compared to the octahedron around yttrium, i.e. B–Na–B < Cl–Na–B < Cl–Na–Cl.

The hydrogen positions determined by DFT optimization show that the BH_4 units act as η^3-ligands coordinating to yttrium via the face corresponding to the cation…H_3B bonding scheme. The three Y–H distances are similar, ranging from 2.312 to 2.382 Å. Thus, taking hydrogen atoms into account, yttrium exhibits 10-fold coordination, i.e. to four Cl and six H (see Fig. 4, left). This situation differs from the 12-fold coordination found in $Y(BH_4)_3$ [41–43,46], where coordination of the BH_4 units only via the edge was observed, as in many other metal borohydrides [17–19]. The coordination via the faces is somewhat unusual, however it has been observed in the hexagonal and the orthorhombic $LiBH_4$ polymorphs [49] and has also been suggested from DFT optimization of the isolated $[Sc(BH_4)_4]^-$ complex observed in $LiSc(BH_4)_4$ [5]. Furthermore it has been suggested from the tentative determinations of hydrogen positions in $MSc(BH_4)_4$ (M = Na or K) [7,8].

The BH_4 units also act as η^1-ligands coordinating via the same vertex to two sodium atoms at Na–H distance of 2.437 Å. In fact, two BH_4 vertices coordinate to the same two Na atoms, making a Na_2H_2 rhomb with H–Na–H angles of 49.54° (see Fig. 4, right). This configuration has not previously been observed in a metal borohydride, however M_2X_2 rhombs are often observed in metal halide structures, as well as in $NaBH_4 \cdot 2H_2O$ where the rhombs are formed both via BH_4 and H_2O [48]. In the Na_2H_2 rhomb in $NaY(BH_4)_2Cl_2$, the H atoms point toward each other resulting in a short H···H distance of 2.042 Å.

The volume of the $NaY(BH_4)_2Cl_2$ formula unit (V/Z = 186.25(2) Å^3) is nearly equal to the sum of the formula volumes for the reactants, YCl_3 (V/Z = 124.2 Å^3) [47] and $NaBH_4$ (V/Z = 58.2 Å^3) [48]. This is also the case for the other known heteroleptic borohydride structure, $KZn(BH_4)Cl_2$ [22]. However, the structure of $NaY(BH_4)_2Cl_2$ exhibits some degree of porosity illustrated in Fig. 3. Relatively large pores are also observed in the structure of the high temperature polymorph of $Y(BH_4)_3$, β-$Y(BH_4)_3$ [41]. This feature is a result of the structure types of these borohydrides, i.e. $MgWO_4$ for $NaY(BH_4)_2Cl_2$ and ReO_3 for β-$Y(BH_4)_3$, which also show some degree of porosity. Interestingly, the structure of $NaY(BH_4)_2Cl_2$ resembles that of the orthorhombic high temperature polymorph of ReO_2 with a small monoclinic distortion [50].

As mentioned, the new sodium yttrium borohydride chloride, $NaY(BH_4)_2Cl_2$ is isostructural to the high temperature polymorph of $NaYCl_4$ (see Fig. 3, right), which is isomorphic to $NaErCl_4$ ($MgWO_4$ structure-type) [38]. The polymorphic phase transition from the triclinic room temperature polymorph (space group P-1) into the monoclinic high temperature polymorph ($P2/c$) of $NaYCl_4$ is reported to occur at ~50 °C [51]. However, the incorporation of BH_4 units into the structure likely facilitates structural expansion similar to thermal expansion due to the larger size of BH_4^- compared to Cl^-. This likely causes the topology of the high temperature polymorph to be stable at RT. Interestingly, a hypothetical structure of $NaY(BH_4)_2Cl_2$ can be built from $NaYCl_4$ by substitution of the Cl by BH_4 units at the Cl2 site only. In order to rationalize this observation further, a hypothetical "$NaYCl_2(BH_4)_2$" structure has been studied by DFT methods, in which all Cl atoms at the Cl1 site in $NaYCl_4$ are replaced with BH_4 units (see Supplementary material Table S5 and Fig. S1). Optimization of this structure by DFT calculation shows that the energy of the final structure is 0.31 eV/f.u. higher and the volume (V/Z = 192.0 Å^3) 1.9% larger than the values for $NaY(BH_4)_2Cl_2$ with BH_4 on the Cl2 site. Thus the DFT simulation supports the experimental structural model showing BH_4 substitution only on the Cl2 site in the isomorphous structure of $NaYCl_4$.

Furthermore, it is found that the Cl2 sites in the discussed structures are larger than the Cl1 sites. In the experimentally determined structural model of $NaY(BH_4)_2Cl_2$ the shortest Cl–Cl distance is 3.376(7) Å while the B–B distance is 3.839(15) Å. The same trend is observed in the ternary chlorides, i.e. in the DFT-optimized $NaYCl_4$ and the experimentally determined $NaErCl_4$ structure the Cl1–Cl1 distances, 3.463 and 3.413 Å, respectively, are much shorter than the Cl2–Cl2 distances of 3.715 and 3.785 Å. Note that the experimental atomic positions of $NaYCl_4$ are not reported. In addition Cl1 in both $NaYCl_4$ and $NaErCl_4$ coordinates to one sodium and two yttrium atoms, while Cl2 coordinates to one yttrium and two sodium atom. As the ionic radius of Na^+ (116 ppm) is larger than that of Y^{3+} (100.8 ppm), this further indicates that the Cl2 site is larger than the Cl1 site. Given the larger size of the borohydride over the chloride anion, it becomes clear why BH_4 occupies the Cl2 site only.

The possibility of Cl substitution on the BH_4 (Cl2) site is studied theoretically by evaluating total energies of $NaY(BH_4)_{2(1-x)}Cl_{2(1+x)}$ solid solutions with x = 0.0, 0.25, 0.5, 0.75, 1.0. The volume of the formula unit, V/Z of $NaY(BH_4)_{2(1-x)}Cl_{2(1+x)}$ and ΔE is plotted as a function of temperature in Fig. 5. The volume per formula unit decreases linearly as x increases, and ΔE turns out to be negative for all selected discrete x values. Three distinct symmetrically independent configurations were optimized for x = 0.5. These

configurations have similar volumes and negative ΔE, however the individual ΔE values scatter somewhat. In conclusion, the DFT calculations suggest possible formation of a solid solution in the entire compositional range $NaY(BH_4)_2Cl_2$–$NaYCl_4$. According to the calculation, the experimentally found value $x = 0.21(3)$ is likely determined by an equilibrium with the chloride substitution in $Na(BH_4)_{1-x}Cl_x$, which exhibits similar degree of substitution ($x = 0.22$ or 0.24), rather than by a limited solubility in $NaY(BH_4)_{2(1-x)}Cl_{2(1+x)}$ itself.

3.3. *Raman and infrared spectroscopy*

In general the infrared and Raman spectra of the $NaBH_4$–YCl_3 samples show signals of both $Na(BH_4)_{1-x}Cl_x$ as well as those of the title compound. Fig. 6 shows the IR spectrums of $NaBH_4$–YCl_3 (4:1) and, for comparison, of a ball-milled $NaBH_4$–NaCl (1:1) mixture. For the latter it has been shown that a $Na(BH_4)_{1-x}Cl_x$ solid solution with $x \sim 0.1$ is formed from ball milling [52]. The band at ~1200 cm^{-1} belongs to $NaY(BH_4)_2Cl_2$, while in the stretching mode region around 2300 cm^{-1}, there appears to be significant spectral overlap. Raman spectra obtained with progressively increasing temperature on both the 3:1 and 4:1 mixtures of $NaBH_4$–YCl_3 show an increase of the bands belonging to $NaY(BH_4)_2Cl_2$, in agreement with the synchrotron diffraction study (see Fig. 8). However, during the Raman measurements the heat treatment was performed during a longer time interval than compared to the *in-situ* SR-PXD experiment, which might explain that a significant larger amount of $NaY(BH_4)_2Cl_2$ is formed at lower temperature in the Raman experiment, i.e. 106 compared to 120 °C observed in the *in-situ* SR-PXD data. Therefore, Fig. 7 shows the difference-Raman-spectrum, i.e. the spectrum measured at 67 °C subtracted from the spectrum measured at 106 °C of the $NaBH_4$–YCl_3 (3:1) sample. This allows suppressing almost completely the contribution of the $Na(BH_4)_{1-x}Cl_x$ solid solution present as a side product. The origin of the sharp band at ~220 cm^{-1} is not clear, however it

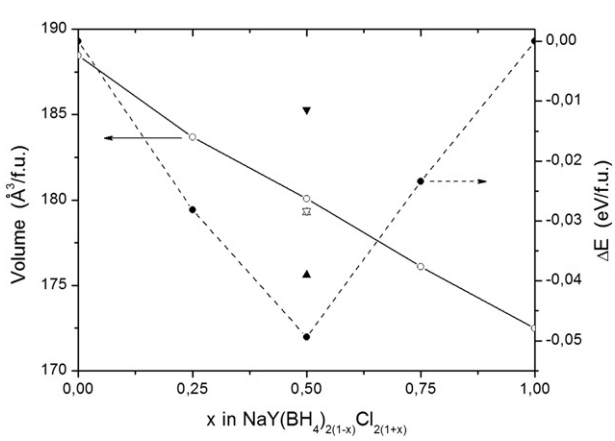

Fig. 5 – Volume per formula unit and energy of $NaY(BH_4)_{2(1-x)}Cl_{2(1+x)}$ as a function of x. Open and filled symbols represent volume and energy, respectively. Three symmetrically independent structures are calculated at $x = 0.5$ and the corresponding volume and energy for each structure are shown using the same shape of symbol.

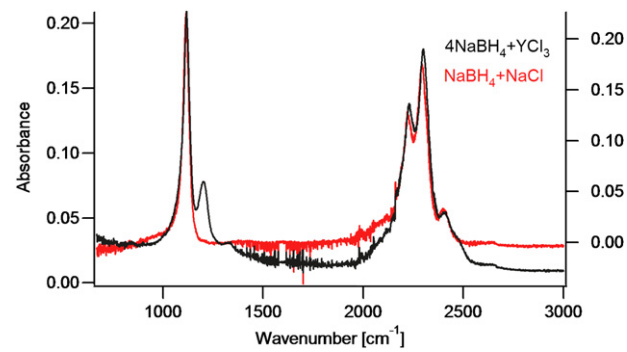

Fig. 6 – IR spectra measured at RT of the $NaBH_4$–YCl_3 (4:1) mixture (black curve) and of a $NaBH_4$–NaCl (1:1) mixture (red curve). (For interpretation of the references to colour in this figure legend, the reader is referred to the web version of this article.)

is most likely arising from Y–Cl vibrations. The Raman spectra reported for YCl_6^{3-} in different hosts show the strong A_{1g} band between 260 and 285 cm^{-1}, while the Raman spectrum of YCl_3 has the strongest band at 256 cm^{-1} [53]. The broader band around 460 cm^{-1} can be assigned to a Y–B stretching motion, similarly to the band seen for $NaSc(BH_4)_4$. A previously reported spectrum of $NaSc(BH_4)_4$ is shown for comparison in Fig. 7 [7]. Some similarities exit around 2200–2500 cm^{-1}, while the bending mode region for the $NaBH_4$–YCl_3 (3:1) sample presents only weak bands. However, the strong IR band at 1200 cm^{-1} (Fig. 6) is comparable to the bands observed around 1190 cm^{-1} in $MSc(BH_4)_4$ with M = Li, Na, K (see Table S4 in the supplemental material of Ref. [8]). These similarities show that the BH_4 units coordinate with three hydrogen atoms to the central yttrium atom, which confirms the hydrogen configuration obtained by the DFT optimization of $NaY(BH_4)Cl_2$. A bidentate binding, as seen for instance in $Li_4Al_3(BH_4)_{13}$ [54], would result in a strong IR band around 1400–1450 cm^{-1}, which is clearly not observed here.

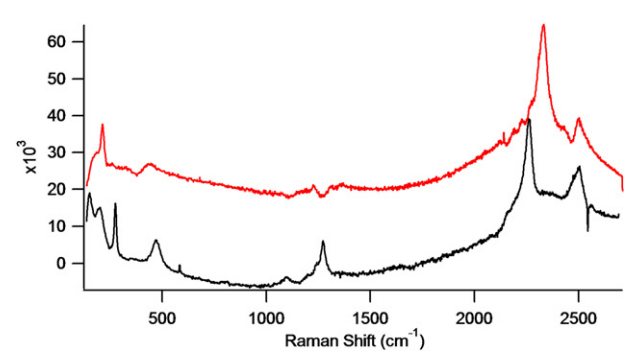

Fig. 7 – Raman spectrum of $NaSc(BH_4)_4$ measured at RT (black curve) and difference curve between the Raman spectra of the $NaBH_4$–YCl_3 (3:1) mixture measured at 106 and 67 °C (red curve). This difference allows for suppression to a significant extent of the bands of the $NaBH_4$–NaCl solid solution. (For interpretation of the references to colour in this figure legend, the reader is referred to the web version of this article.)

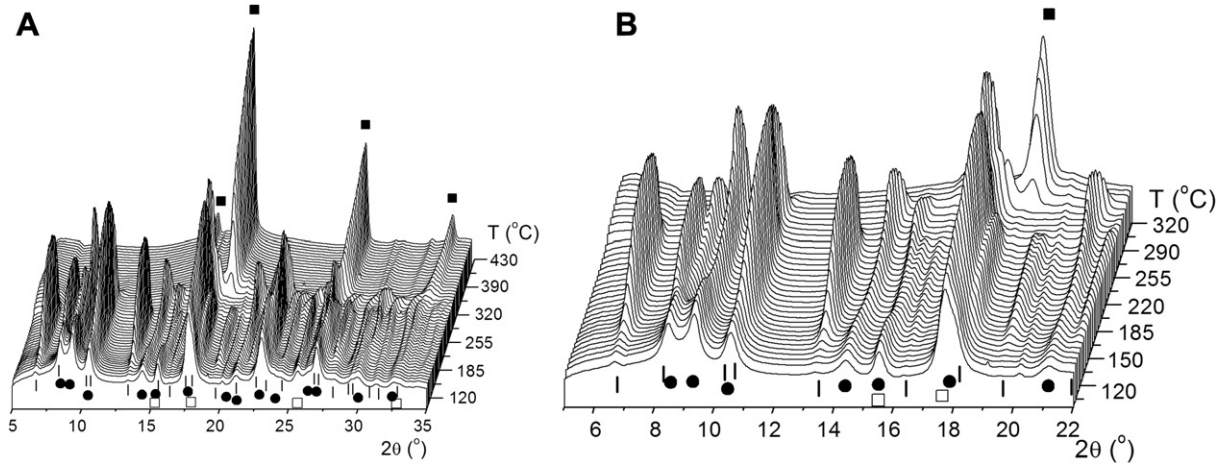

Fig. 8 – *In-situ* SR-PXD data for a ball-milled sample of $NaBH_4$–YCl_3 (3:1) measured from *RT* to 350 °C, $\Delta T/\Delta t = 7$ °C/min. Entire 2θ and temperature range (A) and enlargement of selected data region (B), which shows the crystallization and decomposition of $NaY(BH_4)_2Cl_2$. Symbols: black lines $NaY(BH_4)_2Cl_2$, black circles Na_3YCl_6, white squares $Na(BH_4)_{1-x}Cl_x$ and black squares NaCl ($\lambda = 0.9550$ Å, I711, MAX-lab).

3.4. *Decomposition analysis by in-situ SR-PXD*

The effect of annealing and the thermal decomposition of $NaY(BH_4)_2Cl_2$ was investigated by *in-situ* SR-PXD. The data for the two ball-milled samples of $NaBH_4$–YCl_3 in molar ratios 3:1 (Fig. 8) and 4:1 (Fig. S2) show the same decomposition pathway, however the compound of interest, $NaY(BH_4)_2Cl_2$, was obtained in a higher fraction for the sample with starting composition 3:1.

At *RT* the broad peaks from Na_3YCl_6, $Na(BH_4)_{1-x}Cl_x$ and a small amount of $NaY(BH_4)_2Cl_2$ are observed. No significant changes of the diffraction patterns are observed as the temperature increases from *RT* to 120 °C. Upon further heating the amount and the crystallinity of $NaY(BH_4)_2Cl_2$ increases and reaches a maximum at 230 °C, which was also observed by Raman spectroscopy. This means that the reaction shown in Eq. (1) takes place to a higher extent when induced by heating than by ball milling. Furthermore, the crystallinity of both Na_3YCl_6 and $Na(BH_4)_{1-x}Cl_x$ appears to improve simultaneously, while the degree of substitution, *x* in $Na(BH_4)_{1-x}Cl_x$ increases from 6.4(17)% at *RT* to 24.0(12)% at 230 °C. The latter is most likely due to consumption of $NaBH_4$ and formation of NaCl caused by the ongoing reaction (Eq. (1)). Such a formation and crystallization caused by annealing has not previously been observed for metal borohydrides. This suggests that the synthetic methods based on ball milling in some cases can be complemented by a moderate heat treatment (annealing) in order to obtain novel highly crystalline borohydrides.

At 250–270 °C the diffraction peaks from $NaY(BH_4)_2Cl_2$ decrease abruptly due to a decomposition. In the same temperature range an increase in diffracted intensity from Na_3YCl_6 is observed. This suggests that $NaY(BH_4)_2Cl_2$ decomposes to Na_3YCl_6 and likely amorphous yttrium borides. For $Y(BH_4)_3$, two decomposition pathways were observed: leading to crystalline yttrium hydrides and YB_4 or only to amorphous products, possibly yttrium borides or yttrium boranates with higher boron and lower hydrogen content [41,42]. The later scenario seems to resemble that of the $NaY(BH_4)_2Cl_2$ decomposition.

As the sample is heated to 290 °C the amount of Na_3YCl_6 decreases. Meanwhile, a significant shift in the 2θ position of the Bragg peaks from $Na(BH_4)_{1-x}Cl_x$ is observed, until their position reaches those of NaCl. This suggests that Na_3YCl_6 and $NaBH_4$ react and form NaCl and possibly amorphous products, similar to reactions between M_3ScCl_6 and MBH_4 (M = Na or K) [7,8]. In the temperature range from 290 to 390 °C, diffraction peaks from NaCl increase slowly and hereafter no significant changes are observed. After cooling the sample to *RT* the only decomposition product observed by SR-PXD is NaCl.

3.5. *Thermal analysis*

The thermal decomposition was further investigated on both samples by simultaneous TGA and DSC measurements (see Fig. 9). The slope observed in the DSC data and the continuous small drift in the TGA data are the instrumental artefacts due to buoyancy. Careful inspection of the data reveals small broad signals on the DSC curves around 100–120 °C, which might be due to the ongoing formation of $NaY(BH_4)_2Cl_2$ and suggests that this process is endothermic, as expected. Broad endothermic DSC signals are observed for both samples covering a temperature range from 275 to 350 °C. For the ball-milled sample of $NaBH_4$–YCl_3 (3:1) we observe a single peak with peak temperature at 300 °C. However, for the ball-milled sample of $NaBH_4$–YCl_3 (4:1) this signal consists of several resolved peaks with characteristic temperatures of 292 and 296 °C, followed by a small broad peak at approximately 330 °C. In these temperature regions TGA mass losses are also observed, hence the DSC signals are possibly due to the decomposition of $NaY(BH_4)_2Cl_2$ and the reaction between Na_3YCl_6 and $Na(BH_4)_{1-x}Cl_x$. This reflects that the decomposition temperature of $NaY(BH_4)_2Cl_2$ is close to the average value between the decomposition temperature of $NaBH_4$ (400 °C) and $Y(BH_4)_3$ (190 °C) [9,41]. For the ball-milled sample of

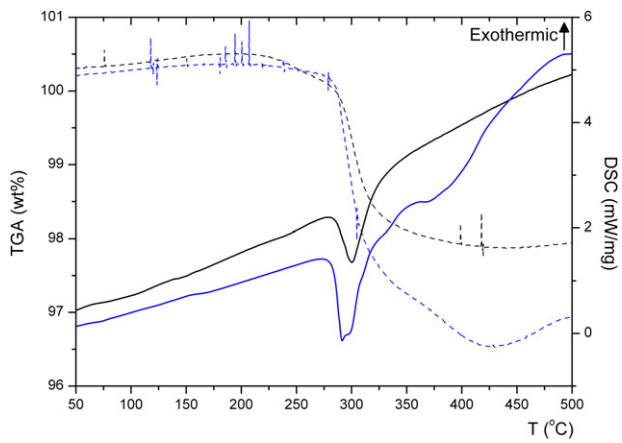

Fig. 9 – TGA-DSC data measure from RT to 500 °C, ΔT/Δt = 10 °C/min for the ball-milled samples of $NaBH_4$–YCl_3 (3:1) and (4:1) shown as black and blue curves, respectively. Solid lines: DSC, dashed lines: TGA. (For interpretation of the references to colour in this figure legend, the reader is referred to the web version of this article.)

$NaBH_4$–YCl_3 (4:1) another broad endothermic DSC signal and a small TGA mass loss of 0.83 wt% are observed in the temperature range from 360 to 425 °C. This might be due to a decomposition of the excess $Na(BH_4)_{1-x}Cl_x$, since this is present in a higher amount in the sample of $NaBH_4$–YCl_3 (4:1) compared to the sample in the starting ratio 3:1. The temperatures for the thermal events are observed to be somewhat higher by TGA and DSC than by *in-situ* SR-PXD, however, this may be owing to the lower heating rate used in the latter type of experiments.

The total observed TGA mass losses are 2.62 and 3.78 wt% for the $NaBH_4$–YCl_3 (3:1) and (4:1) samples and the total calculated hydrogen contents are 3.9 and 4.7 wt%, respectively. The discrepancy may be due to short air exposure prior to TGA measurements, formation of higher boranes, e.g. $Na_2B_{12}H_{12}$ [55–57], presence of minor amounts of $NaBH_4$, either unreacted $NaBH_4$ or $Na(BH_4)_{1-x}Cl_x$ segregated from $NaY(BH4)_2Cl_2$ during heating of the sample.

Formation and release of significant amounts of borane gasses may occur in case the transition metal ions is reduced to the metallic state as observed for all zinc and cadmium based borohydrides [20–25,58], e.g. metallic zinc forms during decomposition of $KZn(BH_4)Cl_2$, which is reported to release 6.5 wt% giving further evidence for release of B_2H_6 since the hydrogen content is only 2.1 wt% [22]. This is not the case for $NaY(BH_4)_2Cl_2$ as no metallic Y is observed in the diffraction data and the observed mass loss is too small to account for release of diborane (the calculated mass loss assuming release of diborane and hydrogen from $NaY(BH_4)_2Cl_2$ is 9.6 and 8.5 wt % for or the $NaBH_4$–YCl_3 (3:1) and (4:1) samples, respectively).

4. Conclusions

A novel mixed-cation mixed-anion borohydride, $NaY(BH_4)_2Cl_2$ has been synthesized and characterized. The synthesis, carried out by ball milling and subsequent annealing, resulted in a number of simultaneous and coupled addition and metathesis reactions leading to formation of not only $NaY(BH_4)_2Cl_2$ but also of Na_3YCl_6 and $Na(BH_4)_{1-x}Cl_x$. Annealing the ball-milled samples at 120–230 °C was found to drastically improve the amount of the title compound and the overall crystallinity. Similar effects on heating have not previously been observed for metal borohydrides and this may provide new synthesis routes of combined ball milling and heat treatment. The crystal structure of $NaY(BH_4)_2Cl_2$ is monoclinic with $\beta \sim 90°$, built by edge- and corner-sharing of octahedral coordination polyhedra of Y ($4Cl + 2BH_4$) and Na ($2Cl + 4BH_4$) atoms. The structure determination was complemented by DFT studies, yielding orientation of the BH_4 unit, acting as a η^3-ligand towards yttrium and as a η^1-ligand towards sodium atoms. This BH_4 configuration was confirmed by Raman spectroscopy. In-situ SR-PXD studies of the decomposition show that $NaY(BH_4)_2Cl_2$ decomposes to Na_3YCl_6 and likely amorphous yttrium borides associated with an endothermic process at $T \sim 300$ °C. The observed TGA mass losses suggest that no significant amount of borane gasses is released during the decomposition, i.e. boron is maintained in the solid state, which is a prerequisite for reversible hydrogen storage in borohydrides.

Acknowledgements

We thank the Danish Research Council for Nature and Universe (Danscatt), the Danish National Research Foundation (Centre for Materials Crystallography), the Danish Strategic Research Council (Centre for Energy Materials), the Swiss National Science Foundation and the Carlsberg Foundation. We are also grateful to the European Synchrotron Radiation Facility, the Swiss-Norwegian Beam Lines and MAX-lab for the provision of beam time. Y.-S.L. and Y.W.C. acknowledge support by Hydrogen Energy R&D Center, one of 21st Century Frontier R&D Programs funded by the Ministry of Education, Science and Technology of Korea.

Appendix A. Supporting material

Supplementary data related to this article can be found online at doi:10.1016/j.ijhydene.2012.02.130.

REFERENCES

[1] Eberle U, Felderhoff M, Schüth F. Chemical and physical solutions for hydrogen Storage. Angew Chem Int Ed 2009;48: 6608–30.
[2] Schlapbach L. Hydrogen-fuelled vehicles. Nature 2009;460: 809–11.
[3] Grochala W, Edwards PP. Thermal decomposition of the non-interstitial hydrides for the storage and production of hydrogen. Chem Rev 2004;104:1283–315.
[4] Orimo S, Nakamori Y, Eliseo JR, Züttel A, Jensen CM. Complex hydrides for hydrogen storage. Chem Rev 2007;107:4111–32.
[5] Hagemann H, Longhini M, Kaminski JW, Wesolowski TA, Černý R, Penin N, et al. $LiSc(BH_4)_4$: a novel salt of Li^+ and

discrete $Sc(BH_4)^{4-}$ complex anions. J Phys Chem A 2008;112: 7551–5.
[6] Purewal J, Hwang S-J, Bowman RC, Rönnebro E, Fultz B, Ahn C. Hydrogen sorption behavior of the ScH_2–$LiBH_4$ system: experimental assessment of chemical destabilization effects. J Phys Chem C 2008;112:8481–5.
[7] Černý R, Severa G, Ravnsbæk DB, Filinchuk Y, d'Anna V, Hagemann H, et al. $NaSc(BH_4)_4$: a novel scandium-based borohydride. J Phys Chem C 2010;114:1357–64.
[8] Černý R, Ravnsbæk DB, Severa G, Filinchuk Y, d'Anna V, Hagemann H, et al. Structure and characterization of $KSc(BH_4)_4$. J Phys Chem C 2010;114:19540–9.
[9] Züttel A, Rentsch S, Fischer P, Wenger P, Sudan P, Mauron Ph, et al. Hydrogen storage properties of $LiBH_4$. J Alloys Compd 2003;356–357:515–20.
[10] Maekawa H, Matsuo M, Takamura H, Ando M, Noda Y, Karahashi T, et al. Halide-stabilized $LiBH_4$, a room-temperature lithium fast-ion conductor. J Am Chem Soc 2009;131:894–5.
[11] Mosegaard L, Møller B, Jørgensen J-E, Filinchuk Y, Cerenius Y, Hanson JC, et al. Reactivity of $LiBH_4$: in situ synchrotron radiation powder X-ray diffraction study. J Phys Chem C 2008;112:1299–303.
[12] Arnbjerg LM, Ravnsbæk DB, Filinchuk Y, Vang RT, Cerenius Y, Besenbacher F, et al. Structure and dynamics for $LiBH_4$–LiCl solid solutions. Chem Mater 2009;21:5772–82.
[13] Rude LH, Filinchuk Y, Sørby MH, Hauback BC, Besenbacher F, Jensen TR. Anion substitution in $Ca(BH_4)_2$–CaI_2: synthesis, structure and stability of three new compounds. J Phys Chem C 2010;115:7768–77.
[14] Lee JY, Lee Y-S, Suh J-Y, Shim JH, Cho YW. Metal halide doped metal borohydrides for hydrogen storage: the case of $Ca(BH_4)_2$–CaX_2 (X = F, Cl) mixture. J Alloys Compds 2009;506: 721–7.
[15] Filinchuk Y, Černý R, Hagemann H. Insight into $Mg(BH_4)_2$ with synchrotron X-ray diffraction: structure revision, crystal chemistry, and anomalous thermal expansion. Chem Mater 2009;21:925–33.
[16] Filinchuk Y, Rönnebro E, Chandra D. Crystal structures and phase transformations in $Ca(BH_4)_2$. Acta Mater 2009;57: 732–8.
[17] Filinchuk Y, Chernyshov D, Dmitriev V. Light metal borohydrides: crystal structures and beyond. Z Kristallogr 2008;223:649–59.
[18] Ravnsbæk DB, Filinchuk Y, Ĉerný R, Jensen TR. Powder diffraction methods for studies of borohydride-based energy storage materials. Z Kristallogr 2010;225:557–69.
[19] Rude LH, Nielsen TK, Ravnsbæk DB, Bösenberg U, Ley MB, Richter B, et al. Tailoring properties of borohydrides for hydrogen storage: a review. Phys Status Solidi 2010;208: 1754–73.
[20] Ravnsbæk D, Filinchuk Y, Cerenius Y, Jakobsen HJ, Besenbacher F, Skibsted J, et al. A series of mixed-metal borohydrides. Angew Chem Int Ed 2009;48:6659–63.
[21] Černý R, Kim KC, Penin N, D'Anna V, Hagemann H, Sholl DS. $AZn_2(BH_4)_5$ (A = Li, Na) and $NaZn(BH_4)_3$: structural studies. J Phys Chem C 2010;114:19127–33.
[22] Ravnsbæk DB, Sørensen LH, Filinchuk Y, Reed D, Book D, Jakobsen HJ, et al. Mixed-anion and mixed-cation borohydride $KZn(BH_4)Cl_2$: synthesis, structure and thermal decomposition. Eur J Inorg Chem; 2010:1608–12.
[23] Friedrichs O, Borgschulte A, Kato S, Buchter F, Gremaud R, Remhof A, et al. Low-temperature synthesis of $LiBH_4$ by Gas–solid reaction. Chem Eur J 2009;15:5531–4.
[24] Friedrichs O, Kim JW, Remhof A, Wallacher D, Hoser A, Cho YW, et al. Core shell structure for solid gas synthesis of $LiBD_4$. Phys Chem Chem Phys 2010;12:4600–3.
[25] Friedrichs O, Remhof A, Borgschulte A, Buchter F, Orimo S-I, Züttel A. Breaking the passivation - the road to a solvent free borohydride synthesis. Phys Chem Chem Phys 2010;12: 10919–22.
[26] Cerenius Y, Ståhl K, Svensson LA, Ursby T, Oskarsson Å, Albertsson J, et al. The crystallography beamline I711 at MAX II. J Synchrotron Rad 2000;7:203–8.
[27] Mammen CB, Ursby T, Cerenius Y, Thunnissen M, Als-Nielsen J, Larsen S, et al. Design of a 5-Station Macromolecular crystallography beamline at MAX-Lab. Acta Phys Pol. A 2002;101:595–602.
[28] Jensen TR, Nielsen TK, Filinchuk Y, Jørgensen J-E, Cerenius Y, Gray EM, et al. Versatile in situ powder X-ray diffraction cells for solid–gas investigations. J Appl Cryst 2010;43:1456–63.
[29] Hammersley AP, Svensson SO, Hanfland M, Fitch AN, Häusermann D. Two-dimensional detector software: from real detector to idealized image or two-theta scan. High Press Res 1996;14:235–48.
[30] Vogel S, Ehm L, Knorr K, Braun G. Automated processing of 2D powder diffraction data. Adv X-ray Anal 2002;45:31–3.
[31] Meyer G, Stenzel F. Ternäre chloride vom typ A_3MX_6. II. Das system $Ag_{3-x}Na_xYCl_6$: synthese, strukturen, ionenleitfähigkeit. Z Anorg Allg Chem 1993;619:652–60.
[32] Boultif A, Louer D. Powder pattern indexing with the dichotomy method. J Appl Crystallogr 2004;37:724–31.
[33] Favre-Nicolin V, Černý R. FOX, free objects for crystallography: a modular approach to ab initio structure determination from powder diffraction. J Appl Crystallogr 2002;35:734–43.
[34] Spek A. PLATON, an integrated tool for the analysis of the results of a single crystal structure determination. Acta Crystallogr A 1990;46:C34.
[35] Kresse G, Hafner J. Efficient iterative schemes for ab initio total-energy calculations using a plane-wave basis set. Phys Rev B 1996;54:11169–86.
[36] Perdew JP, Burke K, Ernzerhof M. Generalized gradient approximation made simple. Phys Rev Lett 1996;77:3865–8.
[37] Blöchl PE. Projector augmented-wave method. Phys Rev B 1994;50:17953–79.
[38] Seifert HJ, Büchel DZ. Ternäre chloride in den systemen ACl/YCl_3 (A = Cs, Rb, K, Na). Anorg Allg Chem 1998;624:342–8.
[39] Rodrigues-Carvajal J. Recent advances in magnetic structure determination by neutron powder diffraction. Phys B 1993; 192:55–69.
[40] Jaron T, Grochala W. Probing lewis acidity of $Y(BH_4)_3$ via its reactions with MBH_4 (M = Li, Na, K, NMe_4. Dalton Trans 2011; 40:12808–17.
[41] Ravnsbęk DB, Filinchuk Y, Černý R, Ley MB, Haase D, Jakobsen HJ, et al. Thermal polymorphism and decomposition of $Y(BH_4)_3$. Inorg Chem 2010;49:3801–9.
[42] Frommen C, Aliouane N, Deledda S, Fonneløp JE, Grove H, Lieutenant K, et al. Crystal structure, polymorphism, and thermal properties of yttrium borohydride $Y(BH_4)_3$. J Alloys Compd 2010;496:710–6.
[43] Sato T, Miwa K, Nakamori Y, Ohoyama K, Li H-W, Noritake T, et al. Experimental and computational studies on solvent-free rare-earth metal borohydrides $R(BH_4)_3$ (R = Y, Dy, and Gd). Phys Rev B 2008;77:104114.
[44] Yan Y, Li H-W, Sato T, Umeda N, Miwa K, Towata S-I, et al. Dehydriding and rehydriding properties of yttrium borohydride $Y(BH_4)_3$ prepared by liquid-phase synthesis. Int J Hydrogen Energy 2009;34:5732–6.
[45] Jaron T, Grochala W. $Y(BH_4)_3$ – an old – new ternary hydrogen store aka learning from a multitude of failures. Dalton Trans 2010;39:160–6.
[46] Lee Y-S, Shim J-H, Cho YW. Polymorphism and thermodynamics of $Y(BH_4)_3$ from first principles. J Phys Chem C 2010;114:12833–7.

[47] Templeton DH, Carter GF. The crystal structures of yttrium trichloride and similar compounds. J Phys Chem 1954;58: 940–4.
[48] Filinchuk Y, Hagemann H. Structure and properties of $NaBH_4 \cdot 2H_2O$ and $NaBH_4$. Eur J Inorg Chem; 2008:3127–33.
[49] Soulié JP, Renaudin G, Černý R, Yvon K. L ithium borohydride $LiBH_4$ I. Crystal Structure J Alloys Compd 2002;346: 200–5.
[50] Magnéli A. Orthorhombic rhenium dioxide: a representative of a hypothetic structure type predicted by Pauling & Sturdivant. Acta Cryst. 1956;9:1038–9.
[51] Seifert HJ. Ternary chlorides of the trivalent late lanthanides phase diagrams, crystal structures and thermodynamic properties. J Therm Anal Cal 2006;83:479–505.
[52] Ravnsbæk DB, Rude LH, Jensen TR. Chloride substitution in sodium borohydride. J Solid State Chem 2011;184:1858–66.
[53] Papatheodorou GN. Raman spectroscopic studies of yttrium (III) chloride–alkali metal chloride melts and of Cs_2NaYCl_6 and YCl_3 solid compounds. J Chem Phys 1977;66:2893–900.
[54] Lindemann I, Ferrer RD, Dunsch L, Filinchuk Y, Černý R, Hagemann H, et al. $Al_3Li_4(BH_4)_{13}$: a complex double-cation borohydride with a new structure. Chem Eur J 2010;16: 8707–12.
[55] Her J-H, Zhou W, Stavila V, Brown CM, Udovic TJ. Role of cation size on the structural behavior of the alkali-metal Dodecahydro-*closo*-Dodecaborates. J Phys Chem C 2009;113: 11187–9.
[56] Caputo R, Garroni S, Olid D, Teixidor F, Surinñach S, Baró MD. Can $Na_2[B_{12}H_{12}]$ be a decomposition product of $NaBH_4$? Phys Chem Chem Phys 2010;12:15093–100.
[57] Ngene P, van den Berg R, Verkuijlen MHW, de Jong KP, de Jongh PE. Reversibility of the hydrogen desorption from $NaBH_4$ by confinement in nanoporous carbon. Energy Environ Sci 2011;4:4108–15.
[58] Ravnsbæk DB, Sørensen LH, Filinchuk Y, Besenbacher F, Jensen TR. Screening of metal borohydrides by mechanochemistry and diffraction. Angew Chem Int Ed; 2012. doi:10.1002/anie.201106661.